Design of liquid cooling cold plate for high performance electric traction module on two-wheeler EV

He Bin[1], Jaydeep Saha[2], Tang Gongyue[1], Sanjib Kumar Panda[2]
[1]Institute of Microelectronics (IME), Agency for Science, Technology & Research (A*STAR), Singapore
[2]Department of Electrical & Computer Engineering (ECE), National University of Singapore (NUS)
He_Bin@ime.a-star.edu.sg

Abstract

Recent progress in the design of drive-train inverters for Electric Vehicles (EVs) predominantly emphasizes the minimization of component sizes while concurrently enhancing power densities. This evolution, though significant in advancing automotive technology, introduces complex challenges concerning thermal management. The presented research in this paper delineates a novel liquid cooling system combining jet impingement and mini-channel methodologies to tackle the specific thermal management issues associated with a SiC MOSFET module. Subsequently, the study employs two distinct optimization techniques to perform design optimization of thermal management system, focusing on critical parameters influencing the manufacturability characteristics of the cooling mechanism. After implementing the optimization process, the "*JF*" performance indicator is improved to a value of 1.92, proving the method's efficacy. Furthermore, the outcomes of the optimization analysis indicate that Bayesian Optimization method embodies substantial promise for future design implementations, characterized by its expeditious and reliable optimization process.

Introduction

Drive-train inverters are integral to the efficiency and power output of Electric Vehicle (EV) drive-trains. The current trajectory in automotive technology is towards the miniaturization of components and increased power densities [1]. The Department of Energy has outlined a future-oriented goal for automotive drive-train inverters, setting an ambitious target of 100 kW/L by 2025, up from the previous goal of 18 kW/L in 2020 [2]. This rapid scaling, however, brings about significant thermal management issues. Rising heat fluxes within Power Electronic (PE) devices can lead to overheating, undermining their effectiveness and reliability, and potentially resulting in failure. Since heat is a primary contributor to PE failure, the integration of an efficient cooling system is imperative to ensure reliability and longevity of the electronics.

Unlike traditional air cooling, liquid cooling methods, employing coolants such as water or glycol-based solutions, circulate through a cold plate in contact with the inverter's heat sink. This technique absorbs heat emanating from the power semiconductor devices and disperses it into the air via a heat exchanger or radiator. Generally, for high-power inverters, liquid cooling surpasses air cooling in cooling capacity. The design of such thermal management solutions must duly consider various factors, including the EV's power level, size, weight, and budget constraints.

The recent shift to a baseplate-less design in PE has decreased both the conduction path and thermal resistance between the junction and the coolant [2]. While this improves efficiency, it may impede heat diffusion, leading to localized hotspots. To combat this issue, cooling methods are integrated as close to the heat source as possible [3]. The Department of Energy's investigations into direct cooling through jet impingement, using dielectric fluid and a pumping power of 0.15 W, have achieved impressive heat transfer coefficients of 17.3 kW/m^{2}K [4]. The results, including the dissipation of 2.15 kW of heat at a maximum junction temperature of 220 °C, are promising. Some researchers also explored methods that employ silicon etching with microchannels directly bonded to the Wide bandgap (WBG) module [5].

Yet, cooling designs employing jet impingement and mini-channel structures are inherently non-linear, and the development process often relies on techniques such as Design of Experiment (DoE) and Response Surface Methodology (RSM) [6]. While extensive research has been conducted through DoE, the focus has been mainly on theoretical optimization rather than practical, manufacturable values for real-world applications like EV drive-train inverter, etc.

In this study, a novel cooling design is proposed that integrates jet impingement and mini-channel techniques to specifically target the localized hotspot issues arising from the new baseplate-less power modules. The approach focuses on directing the jet stream as close as possible to the heat source and introduces a new design optimization process that takes manufacturable values into consideration as constraints.

Methodology

The study presents an optimized design to specifically target hotspot issues, employing localized jet impingement within a water-cooled cold plate. The module selected for this study is the baseplate-less six-switch pack SiC MOSFET module from WolfPACK (CCB021M12FM3), designed to power a two-wheeler by converting 300 V DC to 10 kW @ 180 V AC 3-phase (RMS), 100 Hz. This conversion leads to an internal power loss of approximately 97 W within the module, which is distributed across six SiC transistors as illustrated in Fig. 1.

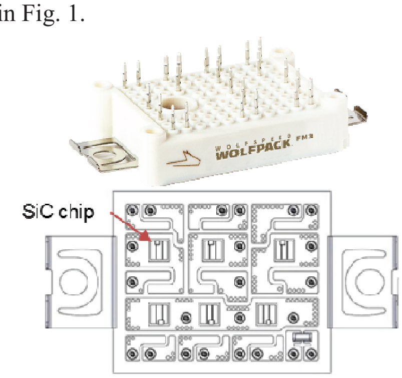

Fig. 1. WolfPACK PE for two-wheeler and SiC chip locations.

The proposed cold plate in focus here is equipped with a distribution plate to divide the flow into dual streams, subsequently directing it to the six SiC chip locations as shown in Fig. 2.(a). This unique design, which involves jet impingement directly over the semiconductor region, maximizes the cooling effect. Following this impingement, the flow is further directed through mini-channels to enhance heat transfer before exiting through the outflow streams. In the case of new power modules, it is possible to simply change the design of the distribution plate, rather than the full cold plate, provided that the new modules have a comparable or smaller footprint. The aggregate volume of the SiC MOSFET module and cool plate is estimated to be roughly 0.04 liters. Furthermore, the baseline design employs a straight fin with a fin to channel ratio of 1:1. However, there is potential for additional performance enhancement by adjusting the fin to channel ratio and making alterations to the fin structures. These modifications are shown in Fig. 2.(b) and will be elaborated further in the subsequent section.

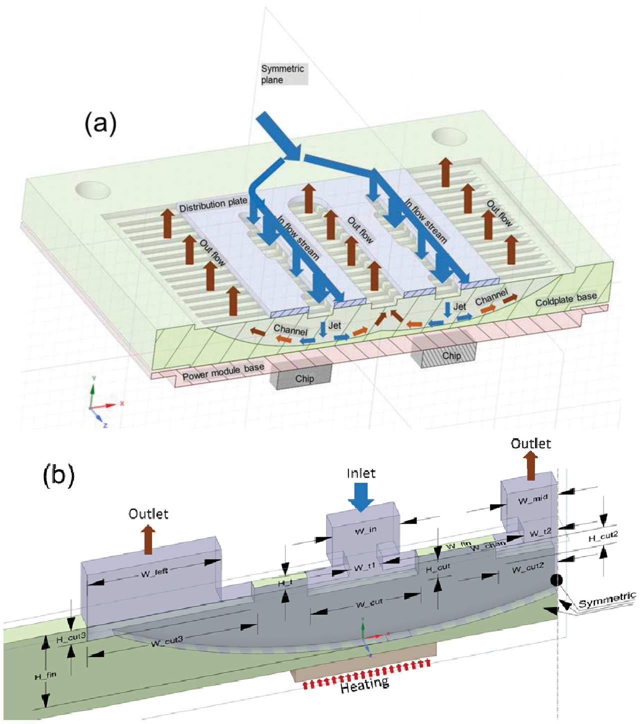

Fig. 2. (a) Cold plate flow arrangement for localized jet flow, (b) Simulation boundary conditions and design parameters

1. *Governing Equations*

The mathematical foundation for this study is laid out through the governing equations specific to a conjugate heat transfer issue within the incompressible steady-state laminar flow regime. It is assumed that the hydraulic and thermal performance of each channel is the same, and the thermal properties of the materials remain constant.

Conservation of mass for liquid region

$$\nabla \cdot \mathbf{u} = 0 \tag{1}$$

Equation of motion for liquid region

$$\rho(\mathbf{u} \cdot \nabla)\mathbf{u} = -\nabla P + \mu_f \nabla^2 \mathbf{u} \tag{2}$$

Energy equation for liquid phase

$$\rho_f c_{p,f} (\mathbf{u} \cdot \nabla) T_f = k_f \nabla^2 T_f \tag{3}$$

Energy equation for solid phase

$$k_s \nabla^2 T_s = 0 \tag{4}$$

where ρ, c_p, k, μ are the density, specific heat, thermal conductivity, and dynamic viscosity, respectively, and subscripts f and s denote fluid and solid phases.

The study has been conducted for constant values of heat flux of 161 W/cm^2 and a total coolant flow rate and inlet temperature of 2 L/min and 50 °C, respectively. The self-similarity of the mini-channel flow enables modeling one channel region from one flow stream, accompanied by half of the channel flow and fin region, applying symmetrical boundary conditions as shown in Fig. 2.(b). Capturing the intricate characteristics of jet impingement necessitates an extensive mesh node, facilitating an accurate representation of the stagnation zone and wall jet flow.

2. *Response Parameters*

The optimization's objective is to strike a balance between heat transfer efficacy and flow resistance within the design constraints. As liquid circulation is facilitated by the pump of the cooling system, the goal is to pinpoint the optimal cooling solution for the given pumping power. The proposal by Yun et al. [7] regarding the *JF* factor method emphasizes the need for an integrated method that takes into account both the larger-the-better heat transfer coefficient and the smaller-the-better pressure drop. This method contributes significantly to the investigation of cooling designs by facilitating the complex evaluation of microchannel performance. The *JF* factor can be used to evaluate the effectiveness of design optimization, which can be derived as follows,

Hydraulic diameter defined as

$$D_h = \frac{2H_{fin}W_{chan}}{H_{fin} + W_{chan}} \tag{5}$$

Reynolds number is defined as

$$\mathrm{Re} = \frac{\rho u_{ave} D_h}{\mu} \tag{6}$$

The convective heat transfer coefficient is:

$$h = \frac{q''}{T_w - T_f} \tag{7}$$

where T_w is the wall temperature, T_f is the bulk temperature of the fluid, and q'' is the heat flux:

The dimensionless surface heat transfer coefficient, i.e., Colburn j factor is defined as,

$$j = \frac{\mathrm{Nu}}{\mathrm{Re} \cdot \mathrm{Pr}^{1/3}} \tag{8}$$

where Nu is the Nusselt number and Pr is the Prandtl number. Friction factor f, respectively, are given by

$$f = \frac{\Delta P}{\frac{1}{2}\rho u^2}\frac{A}{L} \quad (9)$$

Finally, *JF* factor is defined as

$$JF = \frac{j / j_R}{\left(f / f_R\right)^{1/3}} \quad (10)$$

And subscript *R* denotes the values from the reference baseline design.

3. *Numerical Approaches*

The finite volume SIMPLEC algorithm, paired with a pressure-based solver was used to solve the governing equations numerically. A second-order upwind scheme is utilized to discretize the equations pertaining to motion and energy. A thorough grid sensitivity study was conducted on the generated Poly-Hexcore elements, focusing on both hydraulic and thermal response parameters, as listed in Table 1. Extended regions were added to both the inlet and outlet sections of the channel to diminish any entrance and exit effects. Rigorous convergence criteria were set for velocities and continuity at 10^{-5}, and for energy, the threshold was established at 10^{-8}. As observed in Fig. 3, a significant difference in velocity was observed at the intake after the inlet jet. This discrepancy has the potential to substantially impact the accuracy of the simulation pertaining to jet impingement, and therefore, the optimization outcomes. Consequently, in order to precisely represent the high-pressure gradient at the stagnation point resulting from jet impingement and wall jet flow, an additional body-of-influence zone was included into this region of Mesh #3 and Mesh #4. The use of this numerical technique resulted in a notable decrease in the Maximum velocity difference with Mash#4/Maximum velocity (last line in Table 1), reducing it from 31.9 % to 6.5 %. Therefore, Mesh #3 was chosen to be the default configuration for all the cases.

Table 1. Grid independent test, using Mesh #4 as the reference case.

Mesh	#1	#2	#3	#4
Element count	0.42 M	1.52 M	3.39 M	5.91 M
J difference	2.67 %	1.73 %	0.07 %	Ref.
f difference	0.30 %	1.27 %	0.23 %	Ref.
JF difference	2.73 %	1.34 %	0.15 %	Ref.
Max. V. difference / Max. V.	31.9 %	15.0 %	6.5 %	Ref.

The thermal characteristics of the materials used in the present investigation are shown in Table 2. The materials information inside the power module is derived from estimations made using the expertise and sources provided by the vendor of choice.

Optimization Process

1. *Fixed Parameters*

The evaluation of the drive-train inverter in a two-wheeler primarily centers on its potential for commercialization. The design assessment prioritizes the attainment of manufacturability, aiming for low production costs, while also emphasizing the need for excellent cooling performance to achieve a high power-to-volume ratio. Reliability concerns necessitate that the channel size should not be less than 0.5 mm in order to prevent catastrophic thermal runaway caused by cogging. A channel width of 0.5 mm was chosen in order to achieve a balance between those objectives, hence enabling the optimization of design based on the most favorable combination of factors. The aforementioned selections ultimately lead to the selection of a slitting process for the formation of mini-channels on a copper base of 35 mm in length. Additionally, the choice of clean water as the coolant for this operation is mostly based on its widespread availability of data. The coolant selection for commercial vehicles commonly includes WEG50/50, which is supplemented with additives that provide bio-inhibitors and anticorrosion capabilities. However, if comprehensive information about the liquid properties is available, the same optimization procedure can be implemented as well.

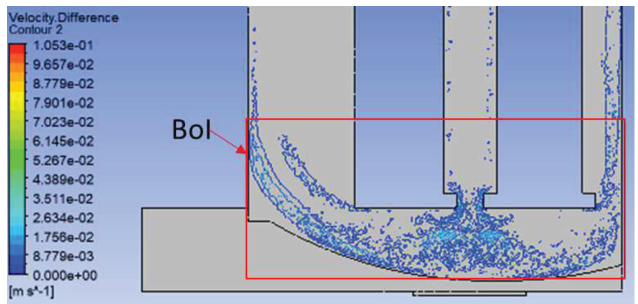

Fig. 3. Discrepancy in coolant velocity between the Mesh #1 and Mesh #4 and the location of the additional body-of-influence (BoI) region

Table 2. Liquid and solid phases properties, density, specific heat, thermal conductivity, and dynamic viscosity, applied in the simulation.

	ρ (kg/m^3)	*Cp* (j/kg • K)	*k* (W/m • K)	μ (Pa • s)
Water @ 50 °C	998.05	4186	0.6406	0.000547
Copper	8978	381	387.6	N.A.
SiC	3216	690	490	N.A.
AlN	3100	700	20	N.A.
TIM	1800	800	5	N.A.
Solder	9000	150	50	N.A.

2. *Optimization Variables*

The optimization process revolves around four types of parameters as follows:

- Number of total fins on the base plate, *nFin*: This parameter impacts overall fin efficiency and heat transfer surface area. More fins will affect the fin's performance and area.
- Width of the jet plate's throat, *Wt1*: This is related to jet strength; a thinner throat increases jet velocity, enhancing

heat transfer but also raising flow resistance. The width is set to range from 0.5-2 mm.

- Height of the slope in the middle outlet, *Hslope*: Influencing the flow resistance and balance between two outlets, this value ranges from 0.1 mm to 0.6 mm.
- Removal of the fin at the inlet and outlet regions, both width and height, inlet: *Wcut* and *Hcut,* outlet at right, *Wcut2* and *Hcut2,* outlet at left, *Wcut3* and *Hcut3,* see Fig. 2. (b): This is related to heat transfer efficiency and flow resistance.

The optimization parameters are summarized in Table 3, and it's worth mentioning that all the parameters, except *nFin*, are normalized to the length of the unit cell (0.5 mm channel and 0.5 mm fin width) in the baseline design to avoid any disproportionality issues.

Table 3. Design parameters and ranges of variation

	nFin	Hslope	Wt1	Wcut	Hcut	Wcut2	Hcut2	Wcut3	Hcut3
Ranges	32 - 45	0.1 - 0.6	1 - 2	0.5 - 2	0.1 - 2.5	0.5 - 2	0.1 - 2.5	0.5 - 2	0.1 - 2.5
Min. step	1	0.1	0.1	0.1	0.1	0.1	0.1	0.1	0.1

3. *Optimization Procedures*

The Design of Experiments combined with Response Surface Methodology has been employed for multi-variable design optimization through multiple trials on experiments. These experiments and trials are typically costly, so the parameters of each trial must be strategically determined to maximize effectiveness. A significant number of factorial trials conducted inside a pre-determined design space are used for the purpose of identifying and differentiating random noise and experimental errors [8].

Unlike classic DoE, the deterministic nature of computer simulation requires a shift in attention towards exploring the design space for a better surrogate model [8]. This can be accomplished by using space-filling methods like Latin hypercube sampling or optimal space-filling methods, aimed at maximizing the distance between sample points. The Krige model may be employed to fit the multi-dimensional space, followed by the application of nonlinear optimization algorithms to obtain optimal solutions to the fitted model. While the detailed process has been extensively explained in existing literature [9], the application of default space-filling methods faces significant challenges.

Most of these methods cater only to continuous design spaces. However, in cases dealing with discrete manufacturable values (as in our study), one must optimize the design in a continuous space and then round these parameters to the nearest manufacturable values. This approach can lead to difficulties, such as when the number of fins cannot take decimal values. Additionally, the theoretical peak might not correspond to a manufacturable value. Consequently, rounding to the next manufacturable value might result in subpar performance compared to the manufacturable peak in the design space, as illustrated in the Fig. 4.

Thanks to advancements in machine learning and Deep Neural Networks (DNN), the process of hyperparameter training now shares similarities with design parameter optimization. Both aim to obtain the best estimation of a "black-box" function's distribution through costly and limited trials without gradient information while seeking the min/max peak of that function. Optimization techniques such as Bayesian Optimization with a Tree-structured Parzen Estimator (TPE) [10] emphasizing uncertainty reduction in the Gaussian Process, have been developed [11]. While providing a good balance between exploration and exploitation, these techniques can handle discrete values, in our case, the manufacturable ones.

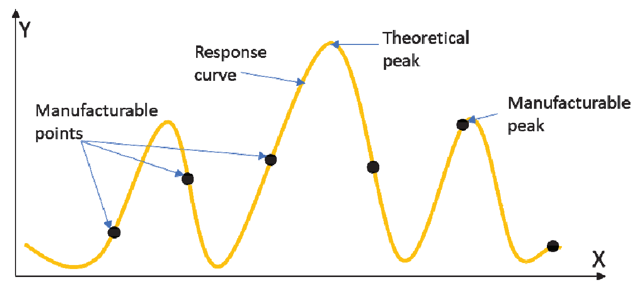

Fig. 4. Schematic explanation of the theoretical peak and the manufacturable peak

The TPE Estimator builds a model using Bayes' rule, expressed through equations (15) and (16), while $p(y<y^*)=\gamma$ [12]. The logic behind these equations is to create two different distributions for the hyperparameters, one for values of the objective function *l(x)* less than the threshold *y** and another *g(x)* for values greater. The Expected Improvement (*EI*) is proportional to the ratio g*(x)/l(x),* and maximizing this ratio leads to the greatest expected improvement.

$$p(x\mid y)=\begin{cases} l(x) & \text{if } y<y^* \\ g(x) & \text{if } y\geq y^* \end{cases} \tag{11}$$

$$EI_{y^*}(x)\propto(\gamma+\frac{g(x)}{l(x)}(1-\gamma))^{-1} \tag{12}$$

In this study, a comparison of two optimization schemes was conducted, each consisting of 147 trials, the same number of samples as that of a corresponding classic Central Composite Design (CCD). The objective is to maximize the value of *JF* within the designated parameter design space. The Krige method was used for the RSM model to represent the DoE approach. In the space-filling design table, the parameter *nFin* was rounded to the nearest integer, which could affect the performance of the RSM model that implies a continuous space, and for simplicity, there was no multi-stage iteration in the RSM. The manufacturable values are implemented only during the peak searching phase. The aforementioned procedures were executed inside the Ansys design explorer, and the optimization process may achieve convergence in about 5 minutes when data from all trials are accessible. In contrast, the novel method utilized Bayesian optimization with TPE samples containing manufacturable values from the outset. This technique can be seamlessly incorporated into an unattended automated optimization process. A Python-based automated optimization process was created using the Ansys pyFluent API, as seen in a flow diagram in Fig. 5.

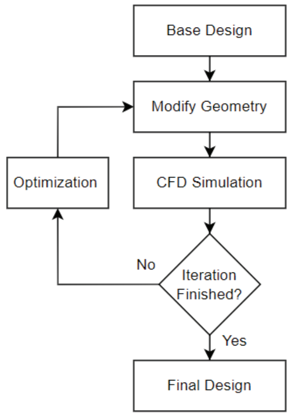

Fig. 5. Schematic of the design optimization workflow with Bayesian optimization

The calculations were performed on an AMD Threadripper 5975WX, with each trial taking approximately 3.5 ± 1 hours. A total of 294 (147+147) groups of trials were conducted. The subsequent sections will detail the findings and implications of these optimizations, providing insights into the most effective designs for the cold plate.

Results and Discussion

The findings presented in Table 4 highlight a significant advancement in the performance metric *JF* from both the DoE and Bayesian optimization methods when compared to the baseline design. The theoretical pumping power, derived from the product of the pressure difference and the volumetric flow rate, is reduced by the DoE method, resulting in a pumping power that is only 11 % of the baseline design. However, this substantial enhancement in flow efficiency is accompanied by a pronounced decrement in thermal performance, evidenced by an increase in temperature differential between junction to ambient, ΔT_{aj} of over 8 °C (43.47 °C to 51.76 °C). It was also observed that this estimated value of *JF* obtained by the DoE technique exhibits a difference of around 22 % when compared to the value derived from the verification trial that have been conducted separately. Despite the high fitness value of 99 % shown, this disparity has the potential to compromise the accuracy of the optimization process. Hence, the use of multi-stage iteration and refinement may be imperative in order to achieve a higher level of granularity in the DoE optimization process. However, it is important to note that this multi-stage methodology would incur additional computing expenses.

Conversely, the Bayesian technique ensures a more balanced outcome. This is evident in Fig. 6 and Fig. 7, where the box with a solid line marks the region of jet impingement and the slash line marks the exits. Both approaches aim to decrease the vertical dimension of the fin situated inside the area of the inlet jet. This alteration facilitates a more vigorous and expedited interaction of the jet with the heat area, leading to a reduced heat transfer pathway. The DoE approach, shown in Fig. 6.(a), involves a significant reduction in the presence of the outlet fin. This reduction aims to facilitate the exit of liquid from the channel and therefore decrease the flow resistance. In contrast, the Bayesian approach, shown in Fig. 6.(b), alters the jet effect by including a slightly taller fin at the inlet, which redirects the flow laterally and therefore decreases energy dispersion from the jet impingement. Additionally, it prolongs the retention of the liquid in the channel, thereby maximizing the utilization of the heat transfer area within the mini channel. These factors contribute to the superior results observed in terms of the ΔT_{aj}. In general, this methodology effectively decreases the energy required for pumping by 87% and leads to a little increase in ΔT_{aj}, of around 5 °C (43.47 °C to 48.56 °C), and a ΔT_{ab} (cold plate base to ambient temperature) of 16.43 °C.

As seen in Fig. *8*, it is worth noting that although not directly comparable, both the sensitivity analysis conducted via DoE and the assessment of parameter importance with Bayesian optimization provide qualitative insights into the approach used for the treatment of parameters in the two optimization techniques. The sensitivity analysis reveals that there are no significant factors, with the exception of a slightly larger value for the removal of fin at the outlet area on the left. The Bayesian methodology places significant emphasis on optimizing jet impingement performance via the manipulation of key parameters such as the jet throat width and the elimination of the fin inside the jet zone. These findings align with the procedures outlined earlier that were used by each optimization strategy. In the broader context of thermal management, the candidate from Bayesian approach offers a superior safety margin, further aligning with applications in driven-train systems. It thereby demonstrates a more favorable trade-off between efficiency and thermal performance.

Table 4. Summary of the base design and two optimization results, DoE (Opt_DoE) and Bayesian optimization (Opt_Bay)

	JF	ΔT_{aj} (°C)	ΔT_{ab} (°C)	Pumping power (W)
Baseline	Ref.	43.47	11.74	0.0257
Opt_DoE	1.89	51.76	19.78	0.0028
Opt_Bay	1.92	48.56	16.43	0.0033

Moreover, an intriguing observation during the optimization process, shown in Fig. 9, is the rapid convergence of the Bayesian method towards an optimal *JF* value of 1.86, reached within 26 trials, and exhibiting only a 3.1 % discrepancy from the maximum value obtained from the full optimization process. Remarkably, this number of trials is even less than the minimum required for a quadric RSM model, as defined by $m(m+1)/2$, where m is the number of design dimension [13]. This highlights the potential of employing the Bayesian method for swift preliminary optimization, providing an efficient pathway for design enhancement.

Conclusions

In summary, this research marks a significant advancement in the field of thermal management for drive-train inverters in commercial two-wheeled electric vehicles. The proposed design introduces localized jet impingement cooling to manage increased heat discharge, culminating in a maximum ΔT_{ab} of 16.43 °C.

The study showcased the innovative integration of a cold plate design. With potential enhancements such as compact PCB design, the total volume could potentially be reduced to less than 0.1 L, surpassing the US Department of Energy's target for power density of 100 kW/L.

The deployment of two optimization methods, particularly the utilization of Bayesian Optimization, stands as a testament to the convergence of artificial intelligence and thermal management. It provides an optimal *JF* result of 1.92 with design space of only manufacturable values. The swift convergence of the Bayesian method highlights the possibility of quick preliminary optimization, emphasizing the practicality of the approach in real-world scenarios.

Furthermore, the cold plate design's inherent adaptability across various drive-train modules opens up avenues for reuse or repurposing in new electric vehicles (EVs), underscoring the sustainable and environmentally friendly aspects of the innovation.

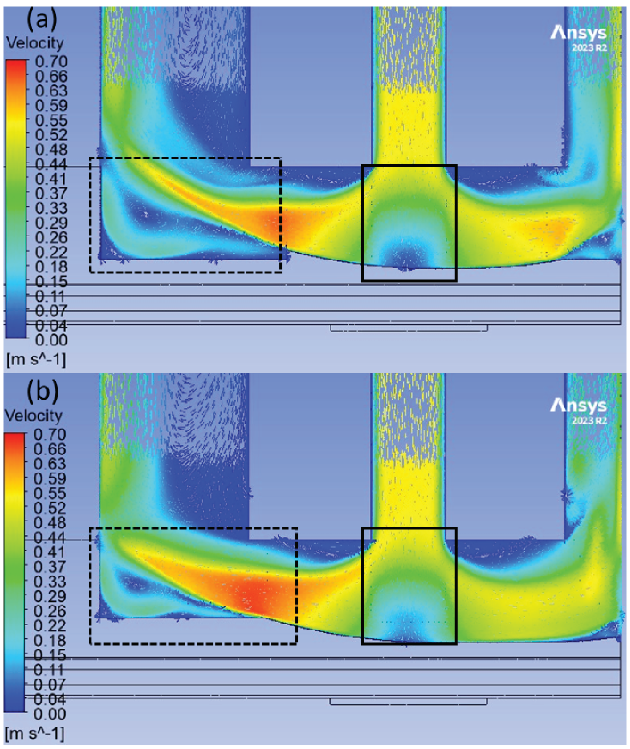

Fig. 6. Computational fluid dynamics simulation results displaying the velocity vector fields, (a) Opt_DoE, (b) Opt_Bay

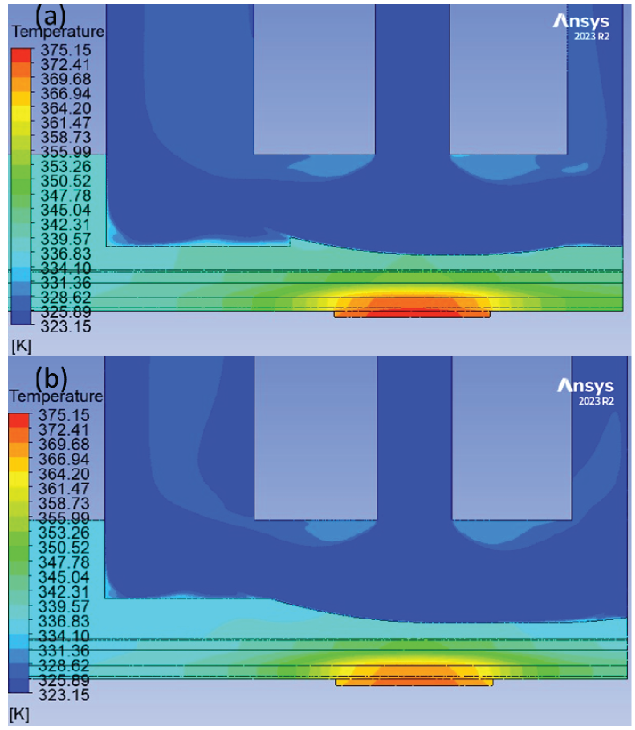

Fig. 7. Computational fluid dynamics simulation results displaying the ΔT (chip to ambient temperature) contours, (a) Opt_DoE, (b) Opt_Bay

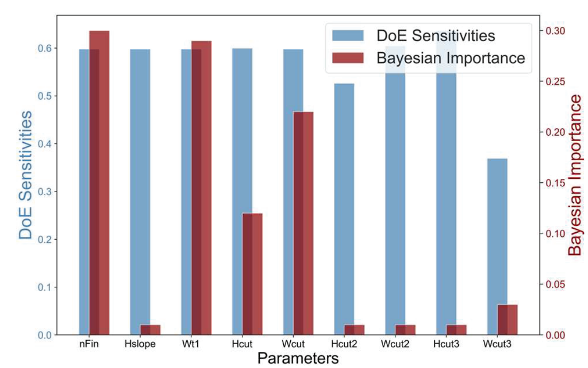

Fig. 8. Results of local sensitivities analysis from DoE v.s. Bayesian importance

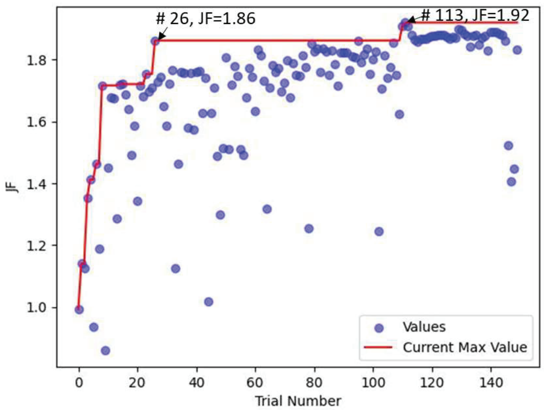

Fig. 9. History of Bayesian optimization process

Acknowledgments

This research is supported by A*STAR under its "RIE2025 MTC IAF-PP: Development of High Performance Electric Traction Module (HiPe-ETraM)", Grant No. M22K4a0044.

References

[1] J. Saha, H. Bin, S. S. Manohar, R. S. Bhujade, T. Gongyue, and S. K. Panda, "A Review on the Design Considerations for Next-Generation e-Motorbike Drive-train Inverter (accepted)," in *Annual Conference of the IEEE Industrial Electronics Society (IECON)*, Singapore, 2023.

[2] S. Jones-Jackson, R. Rodriguez, Y. Yang, L. Lopera, and A. Emadi, "Overview of Current Thermal Management of Automotive Power Electronics for Traction Purposes and Future Directions," *IEEE Trans. Transp. Electrification*, vol. 8, no. 2, pp. 2412–2428, Jun. 2022, doi: 10.1109/TTE.2022.3147976.

[3] M. Liu, A. Coppola, M. Alvi, and M. Anwar, "Comprehensive Review and State of Development of Double-Sided Cooled Package Technology for Automotive Power Modules," *IEEE Open J. Power Electron.*, vol. 3, pp. 271–289, 2022, doi: 10.1109/OJPEL.2022.3166684.

[4] G. Moreno, S. Narumanchi, J. Tomerlin, and J. Major, "Single-Phase Dielectric Fluid Thermal Management for Power-Dense Automotive Power Electronics," *IEEE Trans. Power Electron.*, vol. 37, no. 10, pp. 12474–12485, Oct. 2022, doi: 10.1109/TPEL.2022.3171744.

[5] E. M. Dede, F. Zhou, and S. N. Joshi, "Concepts for embedded cooling of vertical current wide band-gap semiconductor devices," in *2017 16th IEEE Intersociety Conference on Thermal and Thermomechanical Phenomena in Electronic Systems (ITherm)*, May 2017, pp. 508–515. doi: 10.1109/ITHERM.2017.7992529.

[6] Y. Hadad, R. Pejman, B. Ramakrishnan, P. R. Chiarot, and B. G. Sammakia, "Geometric Optimization of an Impinging Cold-Plate with a Trapezoidal Groove Used for Warm Water Cooling," in *2018 17th IEEE Intersociety Conference on Thermal and Thermomechanical Phenomena in Electronic Systems (ITherm)*, San Diego, CA: IEEE, May 2018, pp. 673–682. doi: 10.1109/ITHERM.2018.8419540.

[7] J.-Y. Yun and K.-S. Lee, "Influence of design parameters on the heat transfer and flow friction characteristics of the heat exchanger with slit fins," *Int J Heat Mass Transf.*, 2000.

[8] A. Giunta, S. Wojtkiewicz, and M. Eldred, "Overview of Modern Design of Experiments Methods for Computational Simulations (Invited)," in *41st Aerospace Sciences Meeting and Exhibit*, Reno, Nevada: American Institute of Aeronautics and Astronautics, Jan. 2003. doi: 10.2514/6.2003-649.

[9] X. Song *et al.*, "Surrogate-Based Analysis and Optimization for the Design of Heat Sinks With Jet Impingement," *IEEE Trans. Compon. Packag. Manuf. Technol.*, vol. 4, no. 3, pp. 429–437, Mar. 2014, doi: 10.1109/TCPMT.2013.2285812.

[10] J. Bergstra, R. Bardenet, Y. Bengio, and B. Kégl, "Algorithms for Hyper-Parameter Optimization," in *Advances in Neural Information Processing Systems*, Curran Associates, Inc., 2011. Accessed: Aug. 17, 2023. [Online]. Available: https://proceedings.neurips.cc/paper_files/paper/2011/hash/86e8f7ab32cfd12577bc2619bc635690-Abstract.html

[11] B. Shahriari, K. Swersky, Z. Wang, R. P. Adams, and N. de Freitas, "Taking the Human Out of the Loop: A Review of Bayesian Optimization," *Proc. IEEE*, vol. 104, no. 1, pp. 148–175, Jan. 2016, doi: 10.1109/JPROC.2015.2494218.

[12] T. Akiba, S. Sano, T. Yanase, T. Ohta, and M. Koyama, "Optuna: A Next-generation Hyperparameter Optimization Framework." arXiv, Jul. 25, 2019. Accessed: Aug. 08, 2023. [Online]. Available: http://arxiv.org/abs/1907.10902

[13] Z. Han, "Kriging surrogate model and its application to design optimization: A review of recent progress," *ACTA Aeronaut. Astronaut. Sin.*, vol. 37, no. 11, pp. 3197–3225, Mar. 2016, doi: 10.7527/S1000-6893.2016.0083.